THE JOURNAL OF PHYSICAL CHEMISTRY C

Article

pubs.acs.org/JPCC

Spot Size Engineering in Microscope-Based Laser Spectroscopy

P. Hauer,[†] J. Grand,[‡] A. Djorovic,[†] G. R. Willmott,[§] and E. C. Le Ru*[,†]

[†]The MacDiarmid Institute for Advanced Materials and Nanotechnology, School of Chemical and Physical Sciences, Victoria University of Wellington, P.O. Box 600, Wellington 6140, New Zealand

[‡]Université Paris Diderot, Sorbonne Paris Cité, ITODYS, UMR CNRS 7086, 15 rue J-A de Baïf, 75205 Paris Cedex 13, France

[§]The MacDiarmid Institute for Advanced Materials and Nanotechnology, Departments of Physics and Chemistry, University of Auckland, Auckland 1010, New Zealand

Supporting Information

ABSTRACT: Thanks to the development of microscopy and confocal microscopy, diffraction-limited spot sizes are routinely achieved in spectroscopies such as fluorescence and Raman to achieve submicrometer spatial resolution. Because of their high numerical aperture and collection efficiency, objective lenses are also used in many applications even when a high spatial resolution is not required. In such cases, a diffraction-limited spot size is not necessary and a larger spot may in fact be preferable for a number of reasons, for example, to avoid photodamage, to perform spatial averaging, to ensure a uniform excitation profile, and so forth. In this context, we discuss here simple practical approaches to tailor the spot size with a special emphasis on obtaining large spot sizes with an objective lens. In particular, we demonstrate experimentally that Self's formalism [Self, S. A. *Appl. Opt.* **1983**, *22*, 658] for the transformation of Gaussian beams provides an easy yet powerful approach to predict spot sizes in a typical laser-microscopy setup. A simple practical solution for a continuously tunable spot-size is proposed and studied. These discussions are backed up by experimental measurements in a typical Raman microscopy configuration and further illustrated by practical examples of the use of large spot sizes in the contexts of fluorescence, Raman, and surface-enhanced Raman spectroscopy.

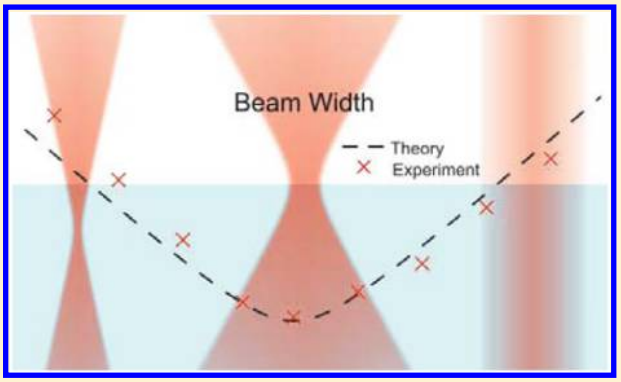

INTRODUCTION

Laser spectroscopies are a common characterization tool in many fields of science from materials and thin films to biology. These include in particular fluorescence and Raman spectroscopy and many variants of these techniques such as fluorescence correlation spectroscopy,[1] time-resolved fluorescence and Raman techniques,[2,3] two-photon fluorescence and hyper-Raman, coherent anti-Stokes Raman spectroscopy (CARS), surface-enhanced fluorescence (SEF), and Raman spectroscopy (SERS).[4−7] These techniques have benefited hugely over the last few decades from technological developments, first of lasers but perhaps more dramatically of CCD array detectors. Microscopy has also become a standard for many fluorescence/Raman setups, and the development of confocal microscopy now allows approximately micrometer resolution in all three dimensions for these optical techniques. For many applications, notably confocal microscopy and high-resolution imaging, a small laser spot size is necessary. It is well understood how such diffraction-limited spot sizes can be achieved by expanding the laser beam to fill the back-aperture of a high numerical aperture (NA) objective.[8] Such considerations are implemented in the design of many fluorescence and Raman spectrometers.[9]

There are however many situations where larger spot sizes are desirable, for example, (i) to decrease the excitation power-density (for example to avoid photodamage[10,11]) without reducing the overall signal, (ii) to ensure a more uniform excitation profile over the area collected by the objective/spectrometer,[11] (iii) to perform spatial averaging without the need for mapping/raster scanning the sample, and (iv) to reduce the large divergence of the exciting beam associated with small spot sizes, for example, in cases where the angular distribution must be precisely controlled, such as the excitation of surface plasmon polaritons[12,13] or angle-dependent spectroscopy.[14] However, a larger spot size means a larger image size at the entrance slit of the spectrometer and therefore worse spectral resolution (or at least a loss in signal if the slits are cutting out some of the image). The choice of spot size is therefore a compromise and must be made on a case-by-case basis. In this context, it is very important to develop tools to predict the spot size and to tune it to any desired target. Simple solutions like changing to a lower magnification objective or

Special Issue: Richard P. Van Duyne Festschrift

Received: May 6, 2016
Revised: July 15, 2016
Published: July 19, 2016

DOI: 10.1021/acs.jpcc.6b04574
J. Phys. Chem. C 2016, 120, 21104−21113

moving the sample away from the focal plane are possible, but they are not ideal as they typically result in large reductions in signal intensity. Other more complicated alternatives have been implemented by some manufacturers, such as line-shaped excitation or the use of scanning mirrors to rapidly raster the position of the laser spot.[15] Those cannot however be easily installed on existing equipment or custom setups.

The focus of this work is therefore to discuss and study simple practical solutions to engineer the size of the laser spot on standard modern spectrometers. An important point is to show how a simple description of Gaussian beam optics as originally described by Self[16] provides a straightforward and effective tool for experimenters to predict beam and spot sizes in many relevant situations. This theory was originally described for ideal Gaussian beams in vacuum.[16] To make it experimentally relevant, it will be generalized here to nonideal beams and to other embedding media to encompass the case of oil- or water-immersion objectives, which are routinely used especially in the life sciences. We show that the resulting Gaussian optics provide accurate predictions of the beam parameters in many experimentally relevant cases and should always be preferred to standard ray optics, which often yield misleading or even wrong conclusions. These assertions are demonstrated using simple examples relevant to common fluorescence and Raman microscopes/spectrometers with a particular emphasis on the practical implementations of larger spot sizes. A particular setup (a Labram HR UV from Horiba Jobin Yvon) is used for demonstration and verification purposes. This work should be valuable to experimentalists using fluorescence or Raman spectroscopy or any of their variants and will allow them to better understand and further optimize their setup to best suit their needs.

METHODS

Properties of a Gaussian beam. We recall here the main parameters defining a Gaussian beam, assumed axisymmetric and propagating along the z-axis (see Figure 1a). Note that we include explicitly in this description the refractive index of the medium, n, and the possibility of a nonideal Gaussian beam (described with the so-called M^2-factor, see below). Using cylindrical coordinates (ρ,z), the intensity is given by

$$I(\rho, z) = I_0\left(\frac{w_0}{w(z)}\right)^2 \exp\left(-\frac{2\rho^2}{w^2(z)}\right) \tag{1}$$

where the z-dependent beam-width and Rayleigh range are defined as

$$w(z) = w_0\left(1 + \left(\frac{z - z_0}{z_R}\right)^2\right)^{1/2} \tag{2}$$

$$z_R = \frac{\pi n w_0^2}{M^2\lambda} \tag{3}$$

with w_0 the beam waist, positioned in the plane $z = z_0$ (i.e., z_0 marks the position of the center of the Gaussian beam). λ is the wavelength in vacuum and n the refractive index of the medium. M^2 in eq 3 is the beam quality factor, which is a measure of how close a laser is to an ideal Gaussian (single mode TEM_{00}) beam.[17] M^2 can be derived from w_0, λ and the far field divergence θ_0 of the beam (defined as $\theta_0 = \lim_{z\to\infty} w(z)/z = w_0/z_R$) as

$$M^2 = \frac{n\pi w_0\theta_0}{\lambda} \tag{4}$$

In practice w_0, θ_0, and therefore M^2 are either known (supplied by the laser manufacturer) or can be measured experimentally.[17] For an ideal Gaussian beam, M^2 becomes 1 but is larger than 1 for a real beam, typically between 1 and 1.1 for He−Ne lasers, in the range of 1.1 to 1.7 for ion-gas lasers, and can reach values as high as 10 for high energy multimode lasers.

The full expression for the electric field can be found elsewhere[18] but will not be necessary here. The intensity has a Gaussian profile in the radial direction and a Lorentzian profile in the axial direction. The power density at the center can be obtained from the measurable optical power P carried by the beam

$$I_0 = \frac{2P}{\pi w^2} \tag{5}$$

Note that the quantity $2w(z_1)$ is usually referred to as the "spot size" in the plane $z = z_1$; the spot size at focus is then $2w_0$.

Self's Formalism for Gaussian Beam Transformation. The transformation of a Gaussian beam as it passes through one or more optical elements can be calculated in the paraxial approximation via the so-called ABCD matrix formalism.[18] A remarkably simpler description was developed by Self,[16] who considered the transformation of the position of the beam center and its waist and obtained an expression similar to the standard thin-lens equation.[19] We here recall the main results with minor modification to encompass the more general case of nonideal Gaussian beams and nonunity refractive indices. We denote f_0 as the (free-space) focal length, f and f' as the object and image focal lengths in the media with refractive indices n and n', and s and s' as the object and image positions along the axis with respect to the lens. For Gaussian beams, these positions refer to the beam centers (see Figure 1b). The equivalent to the thin-lens equation then reads

$$\frac{n}{s + \frac{z_R^2}{s - f}} + \frac{n'}{s'} = \frac{1}{f_0} = \frac{n}{f} = \frac{n'}{f'} \tag{6}$$

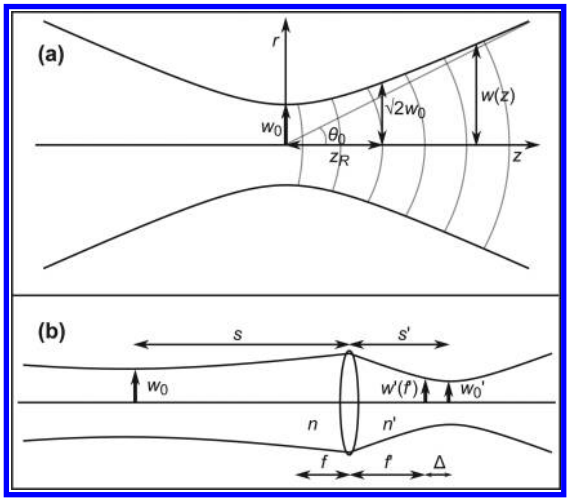

Figure 1. (a) Schematic of the parameters of a Gaussian beam: beam waist at center w_0, beam width $w(z)$, beam divergence θ_0, and Rayleigh range z_R. The wavefronts are indicated by gray lines. (b) Parameters for the transformation of a Gaussian beam across a thin lens.

DOI: 10.1021/acs.jpcc.6b04574
J. Phys. Chem. C 2016, 120, 21104−21113

The usual convention of positive f_0 values for converging and negative f_0 values for diverging lenses applies. Equation 6 is only a slight modification of Self's original equation, which used the assumption that the medium on each side of the lens is vacuum or air with a refractive index of 1. It should however be stressed that in conjunction with eq 3, it can now also be applied to nonideal Gaussian beams with $M^2 > 1$. In most cases of interest, only n' may be nonunity and we will therefore take $n = 1$ and $f = f_0$ in the following. The normalized object distance is then given after simplifications by

$$\frac{s'}{f} = n'\left(1 + \frac{\frac{s}{f} - 1}{\left(\frac{s}{f} - 1\right)^2 + \left(\frac{z_R}{f}\right)^2}\right) \tag{7}$$

The magnification m is the ratio of image-to-object beam waists, explicitly

$$m = \frac{w_0'}{w_0} = \frac{1}{\sqrt{\left(1 - \frac{s}{f}\right)^2 + \left(\frac{z_R}{f}\right)^2}} \tag{8}$$

therefore m is not dependent on n'. We also note that the far-field divergence and the Rayleigh range of a Gaussian beam transform are

$$n'\theta_0' = \frac{\theta_0}{m} \tag{9}$$

$$\frac{z_R'}{n'} = m^2 z_R \tag{10}$$

and the optical invariant $\theta_0\, w_0\, n = \theta_0' w_0' n'$ is conserved, along with the beam quality factor M^2, as expected. Note that the formulas of geometric optics are recovered by taking $z_R = 0$ (i.e., spherical wave-fronts). The pole that normally appears in geometric optics for $s = f$ is here removed by the term $(z_R/f)^2$, which implies that the image distance cannot become infinite. Also, for a laser beam with its waist located at the object focal plane of a convex lens ($s = f$), the waist of the emerging beam is located at the image focal plane of the lens ($s' = f'$). This is to be contrasted with geometric optics where the image would be at infinity (i.e., the image beam would be collimated).

Equations 7, 8, and 9 allow one to calculate the beam properties as it propagates through any set of lenses. They are simple enough to be computed using for example straightforward spreadsheet-based calculations and for convenience, editable spreadsheets implementing Self's formula are provided as Supporting Information for a single objective lens and general two- or three-lens combinations (see Section S.I. of Supporting Information for additional details). The expected range of validity of Self's formalism is the same as that of the paraxial approximation; it is expected to fail for highly divergent, tightly focused beams, typically for $w_0 \leq 2\lambda/\pi$. It is also assumed that the lenses do not significantly clip/aperture the beam. For these reasons, this formalism should not be applied to study diffraction-limited spots or confocal microscopy systems. However, we shall see that they are ideal for many other experimentally relevant situations.

Experimental Section. All measurements were carried out on a Labram HR UV Raman spectrometer (Horiba Jobin Yvon) equipped with an Olympus BX41 microscope setup in a backscattering configuration with a liquid-nitrogen-cooled CCD for Raman (see Section S.II. of Supporting Information for additional details). Several Olympus objectives with magnification ranging from ×10 to ×100 were used. Thanks to a beam splitter in the collection path, the image focal plane can be imaged onto an additional CCD camera located at the focal plane of a 100 mm-focal lens. Extra care was taken to ensure that this imaging camera was located exactly in the focal plane of the lens.

A Melles-Griot Ar^+-ion head operated at $\lambda = 514$ nm was used for all measurements (Raman and beam characterization). For a typical laser like a HeNe or Ar^+-ion laser, the beam can be closely approximated by a Gaussian beam whose center is located inside or close to the exit of the laser cavity. For modeling, we used the beam properties supplied by the manufacturer: $w_0 = 360$ μm and $\theta_0 = 0.5$ mrad from which we deduced $M^2 \sim 1.1$ and $z_R = 720$ mm. The distance from the laser output (assumed to be the Gaussian beam center) to the objectives (fixed on the turret) is estimated to be 1560 mm. The validity of those parameters is justified a posteriori by the general agreement between theoretical predictions and experimental measurements.

Measuring the Beam Width. Experimentally, the width of a laser beam after the objective, and to a degree its intensity profile, can be measured with the "scanning-knife method" (or "edge-scan" technique).[20] The laser beam is scanned laterally perpendicularly and across a sharp edge of a uniform sample, and the signal from the sample surface (which may, for example, be fluorescence or Raman) is measured as a function of displacement. It has to be ensured that the signal originates mostly from the top surface of the sample and that any pinhole or slits used in the detection optics are sufficiently open so that the collection path is not apertured. Assuming an axi-symmetric Gaussian beam profile as given in eq 1 and measured at an axial position $z = Z$, the displacement-dependent intensity $I(x)$ of the signal is then given by

$$I(x) = \frac{I_0}{2}\left(1 + \mathrm{erf}\left(\frac{\sqrt{2}\,(x_0 - x)}{w(Z)}\right)\right) \tag{11}$$

where x_0 denotes the position where the edge is in the middle of the beam, I_0 is the maximum intensity, and erf is the error function.

For this work, we used a silicon sample (for which the penetration depth at 514 and 633 nm is under 1 μm) and registered the Raman intensities as a function of the edge position. The measured $I(x)$ was fitted with eq 11 to obtain the beam waist $w(Z)$ in the plane of measurement. Figure 2 shows the data and the fit for such a measurement. The edge-scan method can in principle be used to obtain the beam width at any desired axial position Z of the beam (see examples later). One should however ensure that optical detection of the signal is not apertured, which can be assessed by closing the slits/pinhole in the detection path. If the beam is too wide or the sample plane too far from the collection objective focal plane (how much depends on the details of the collection path), then the method no longer works. This method was used for all beam width and beam profile measurements of the beam after the objective lens in this work. It is simple and easy to implement but its accuracy decreases for small spots and cannot be used for beam widths smaller than ~2 μm.[21] This limitation is primarily due to larger divergence of the beam (that can therefore excite the sample from the side) and the quality of the cleaved edge.

DOI: 10.1021/acs.jpcc.6b04574
J. Phys. Chem. C 2016, 120, 21104−21113

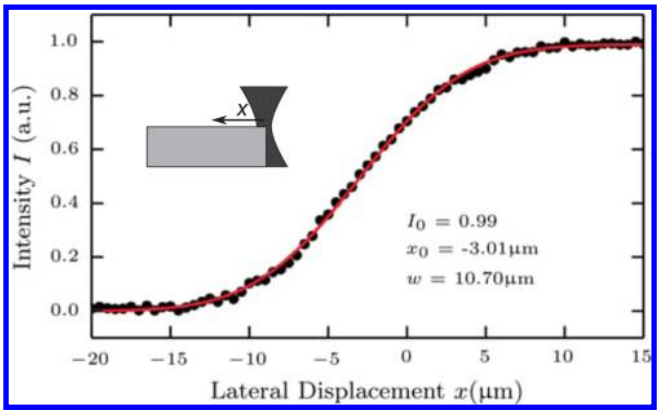

Figure 2. Demonstration of the edge-scan method. Integrated Raman intensity (symbols) of the 520.5 cm^{-1} mode of a silicon sample positioned at the focal plane of a ×10 Olympus objective as a function of the lateral displacement perpendicular to the sample edge. The red line is the fit obtained with eq 11.

RESULTS: THEORETICAL PREDICTIONS AND EXPERIMENTAL VERIFICATION

Focusing of a Laser Beam by a Single Lens. To demonstrate the usefulness of Self's formalism in a practical context, we first use the simple example of focusing a laser beam with a microscope objective. In this case, the most commonly used expression for the focused spot size is

$$2w_0' = \frac{4f\lambda}{\pi 2w(z_{\text{lens}})} \tag{12}$$

where $2w(z_{\text{lens}})$ is the spot size of the incoming beam at the lens position. This expression can in fact be derived directly from eq 8 with the assumption $z_R \gg f$ (which implies $w(z_{\text{lens}}) \approx w_0$). This assumption is often valid in a typical laboratory situation, where one works with a single objective lens with a short focal length, but Self's formalism would enable one to predict the spot size beyond this approximation.

A perhaps less intuitive but arguably equally important property is the location of the focused spot along the axis. For an incident collimated beam, one may expect that the image forms at the focal plane of the objective ($s' = f'$). But for a Gaussian beam, this will only occur if $s = f$ (see eq 7), that is, if the Gaussian beam is centered at the back focal plane (see Figure 3a), in stark contrast with geometric optics. In most cases of interest, the laser is much further away from the objective and eq 7 predicts that the center of the image beam will be beyond the focal plane.

For example, in our spectrometer we estimate the laser beam center to be ~1560 mm away. For a ×50 Olympus objective in air ($f = f' = 3.6$ mm), the image center is then predicted at $s' = f' + 6.9\ \mu$m (see Figure 3b). This offset $\Delta = 6.9\ \mu$m may appear small but because of the tight focusing it makes a big difference: although the beam width at the offset image beam center ($z = f' + \Delta$) is $w_0' = 0.76\ \mu$m, it is more than twice as big at the actual focal plane of the objective ($z = f'$) where $w' = 1.8\ \mu$m. Similar conclusions are obtained with a lower magnification objective, such as a ×20 ($f = f' = 9$ mm) for which an offset of $\Delta = 43\ \mu$m is predicted. It is interesting to note that the predicted beam width at the objective focal plane $w'(f')$ is always $\theta_0 f$, independently of n' and of the laser position.

To demonstrate the validity of theoretical predictions based on the Self's formalism, we have measured the image beam profile in the case of a ×10 objective (where the beam size is larger and the measurement is more accurate). Those experimental results are compared to the theoretical predictions in Figure 3c and demonstrate clearly the validity of the predicted beam sizes and of the offset in focus. In fact, using the microscope eyepiece or an imaging CCD camera, one can in principle easily measure this offset Δ by comparing the positions of the "white light focus" (at which an object is in focus under diffuse white light illumination) with the "apparent laser focus" (at which the laser spot appears smallest). As explained in Section S.III. of the Supporting Information,

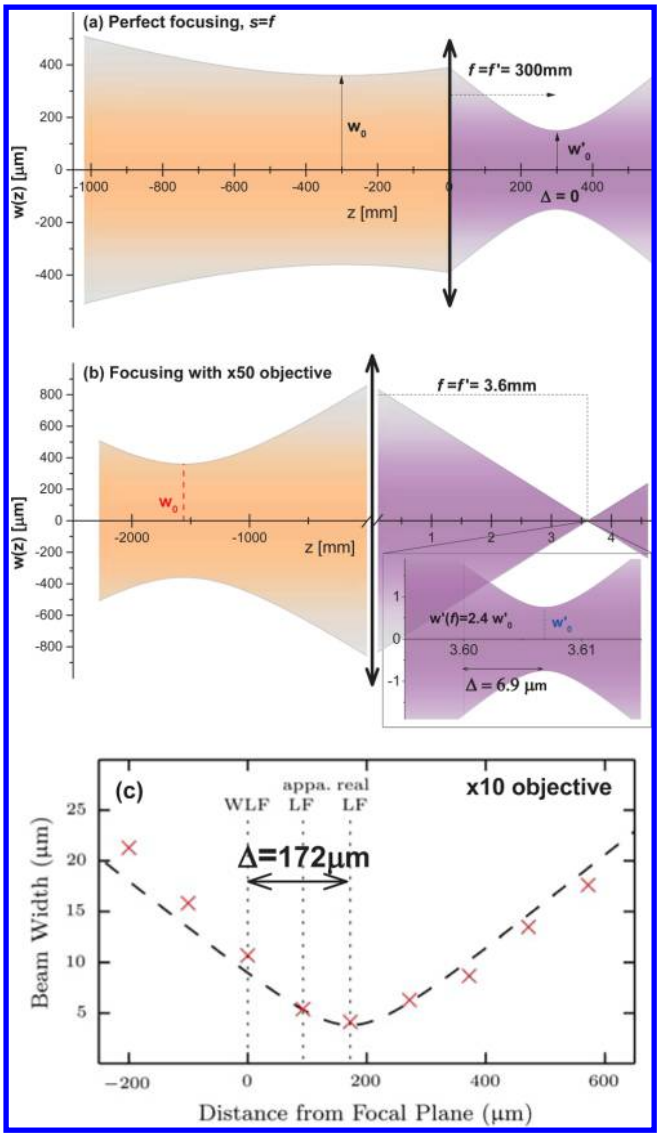

Figure 3. Application of Self's formalism to the focusing of our Ar^+-ion laser ($\lambda = 514$ nm, $w_0 = 360\ \mu$m, $\theta_0 = 0.5$ mrad) on relevant examples. To ensure that the image beam center coincides with the lens image focal plane, the incident laser beam center must be located at the object-focal plane of the lens (a). This is not the case in most situations, and there is an offset between laser focus location and image focal plane, as shown in (b) for a laser 1560 mm away from the objective. In (c), the theoretical predictions (line) are compared to the measured beam profile (symbols) after focusing through a ×10 Olympus objective. The location of the planes for "white light focus", "apparent laser focus", and "real laser focus" are indicated as dotted lines (see Section S.III. of Supporting Information for additional details on those planes).

DOI: 10.1021/acs.jpcc.6b04574
J. Phys. Chem. C 2016, 120, 21104−21113

providing the imaging path is correctly aligned/conjugated, this distance is $\Delta/2$ when using a reflective sample like silicon because the "real laser focus" does not coincide with the "apparent laser focus". Using this technique and the beam size measurement technique described in the Methods, the offset Δ and beam waist at the objective focal plane $w'(z = f')$ were measured and compared to predictions for several objectives as summarized in Table 1. The good agreement suggests that

Table 1. Calculated and Measured Properties for Our Ar^+-Ion Laser Focusing through Different Objectives: Beam Width at the Image Focal Plane $w'(z = f')$ and Offset Δ between the Objective Image Focal Plane and the Focused Spot (Center of the Focused Beam)[a]

objective	$w'(f')$ (μm) theor/meas	Δ (μm) theor/meas
×10	9.00/10.70	172/183
×20	4.50/4.78	43/34
×20imm	4.50/5.06	57/64
×50	1.80/–	6.9/6.7
×100	0.90/–	1.7/1.7
×100imm	0.90/–	2.3/3

[a]Note that small spot sizes could not be measured with the edge-scan technique.

Self's formalism is a powerful tool to predict those effects. Those figures obviously depend on the laser location and its beam properties and should be computed on a case-by-case basis (for example, using spreadsheets provided as Supporting Information).

This offset and the resulting difference in spot size between the focused spot and the image focal plane can be problematic in the most common backscattering configuration, where the signal is collected with the same objective lens as used for excitation. If the experimenter positions a sample at the image focal plane, then the spot area is much larger (by a factor of 5.6 with the ×50 objective here) than would be naively expected from the standard spot size formula (eq 12). If the slits are large enough not to clip the larger image, then this may not be obvious from the signal intensity (which is the same because it is usually integrated over the spot size area) but it would result in a lower spectral resolution and could have other undesirable effects if the signal is not linear with power density, for example, in the presence of photodegradation/photobleaching. If the sample signal originates from a well-defined thin region (for example, the surface of a silicon substrate excited in the visible), one may instead position the sample at the focused beam center (i.e., at $z = s' = f' + \Delta$), but the offset could then result in a reduced signal and image distortions because collection is not optimum if the light does not originate from the focal plane.

Alternatively, as the sample is usually positioned at the focal plane of the objective, additional optical elements can be added in the beam path to tailor the spot location (and possibly its size). In confocal microscopes, this is solved by adding two lenses and a pinhole in the excitation path. With an adequate choice of lenses, this moreover allows the spot size to be reduced close to the diffraction limit, where Self's formalism is no longer valid and a more elaborate description is necessary.[22] Here we will instead discuss the opposite but equally important limit where an expanded spot size is required at the objective focal point.

Using a Back-Focal-Plane Lens. As explained in the Introduction, expanded spot sizes are useful in a number of contexts. There are at least two straightforward ways to change the spot size. The first is to change the objective lens magnification but any increase in spot size is then at the expense of a decrease in the numerical aperture and therefore of the overall collected signal. For solid samples with a thin active layer, one may also move the sample out of focus but this typically means that the sample is no longer at the focal plane, which again can be detrimental to the signal intensity and imaging quality. Moreover, this does not work for liquids, gases, or weakly absorbing solids. We will therefore concentrate in the following on two endeavors

- Case A: How to change/tune the beam width at the focal plane of the objective lens, i.e. $w'(z = f')$, irrespective of where the beam focuses. This easier case will only be relevant to solid samples with a thin active layer, typically the surface of a strongly absorbing sample like silicon in the context of Raman.
- Case B: For liquids, gases, or weakly absorbing solids, we aim to ensure that the focused beam center coincides with the image focal plane, that is, that $s' = f'$ or equivalently $\Delta = 0$, while retaining the ability to change the image beam waist $w'_0 = w'(z = f')$.

Both cases will require the addition of new lenses in the optical path before the objective. There may also be additional experimental constraints limiting the possible positions of those lenses. For example, in many practical setups, there is a minimum possible distance between additional lenses and the objective lens because of filtering elements that must be located in the collection path only (notch-filter for Raman, or band-pass-filter for fluorescence). This minimum distance is 600 mm in our system and we will therefore enforce it in the examples given below. Again the spreadsheets provided as Supporting Information can be used to adjust predictions to other setups.

One intuitive approach to increase the spot size is the use of a lens (called back-focal-plane lens, BFPL) to focus the incident laser beam on the back-focal-plane of the objective.[12] Geometric optics then suggests that the beam after the objective is collimated and therefore has a low divergence and a large spot size. Naively, a $f_B = 600$ mm focal lens placed at $z_B = -603.6$ mm before the ×50 objective with $f = 3.6$ mm would result in a focused spot at the back focal plane in which case the image would be a perfectly collimated beam and result in a strongly expanded laser spot. Again, the Gaussian nature of the beams affects those conclusions and Self's formalism can be used to obtain more accurate predictions, as illustrated in Figure 4 for the same laser properties as used earlier for Figure 3. We see that a shorter focal length of $f_B = 460$ mm (still located at $z_B = -603.6$ mm) is in fact necessary for case **B** to compensate for the (very mild) divergence of the incident beam and achieve $s' = f'$, that is, focus at the image focal plane.

While having $s' = f'$ is an improvement, the goal of increasing spot size is not as successful: the beam width at the image focal plane is less than 2 times larger than without the BFPL (where we had $w'(z = f') = 1.8$ μm). If the condition $s' = f'$ is relaxed (case **A**), one may then replace the BFPL with an even shorter focal lens (called a wide field lens, WFL), for example, $f_B = 300$ mm still located at $z_B \approx -600$ mm. The laser will then be focused beyond the optical plane to a small spot but due to its high divergence, the beam width is large at the objective focus. To further demonstrate the validity of Self's formalism in those contexts, beam widths at the focal plane were measured with either a BFPL or a WFL for three different objectives and again

DOI: 10.1021/acs.jpcc.6b04574
J. Phys. Chem. C 2016, 120, 21104–21113

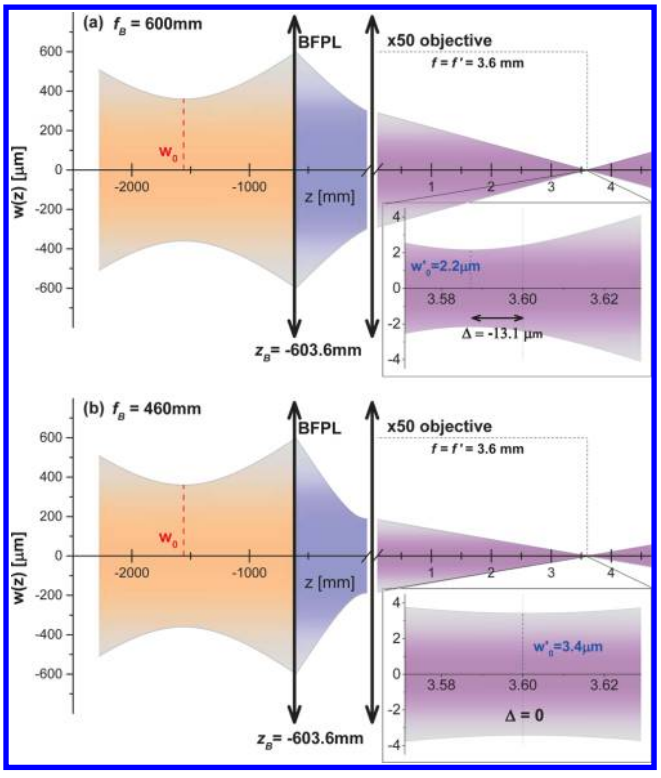

Figure 4. Application of Self's formalism to the use of a back focal plane lens. Examples of a BFPL located 603.6 mm away from the ×50 objective in air (with $f = f' = 3.6$ mm). Although ray optics for a collimated laser beam would suggest to use a focal length of $f_B = 600$ mm (a), a larger spot size and nonoffset focus is in fact obtained with a shorter focal length of $f_B = 460$ mm (b).

there is good agreement with predictions as summarized in Table 2.

Table 2. Calculated and Measured Beam Width at the Focal Plane of Several Objectives in Combination with a Lens of Various Focal Lengths (~500 mm for BFPL, ~300 mm for WFL) Positioned at a Distance ~600 mm from the Objective Lenses

objective	lens	$w'(f')$ (µm) theor/meas
×10	BFPL500	15.38/13.01
×10	WFL300	29.30/27.55
×20	BFPL500	7.69/6.03
×20	WFL300	14.65/12.64
×20imm	BFPL500	7.69/6.25
×20imm	WFL300	14.65/13.24

In order to obtain both a larger spot size and a focus exactly on the image focal plane (case B), one would need to use a shorter focal BPFL closer to the objective. This is not possible in our experimental setup but we will relax this constraint here for illustration purposes. For a given focal f_B, and fixed laser-to-objective distance (1560 mm for us), we use Self's formalism to determine the BFPL position z_B that ensures coincidence between the image beam center and objective focal planes (i.e., $\Delta = 0$). Those BFPL positions, along with the resulting beam waist ($w'(z = f') = w'_0$) are plotted in Figure 5 for a ×50 objective ($f = f' = 3.6$ mm). A waist of $w'_0 = 12$ µm can then, for example, be obtained with a $f_B = 200$ mm lens located at $z_B = -230$ mm. This graph is a vivid example of how Self's

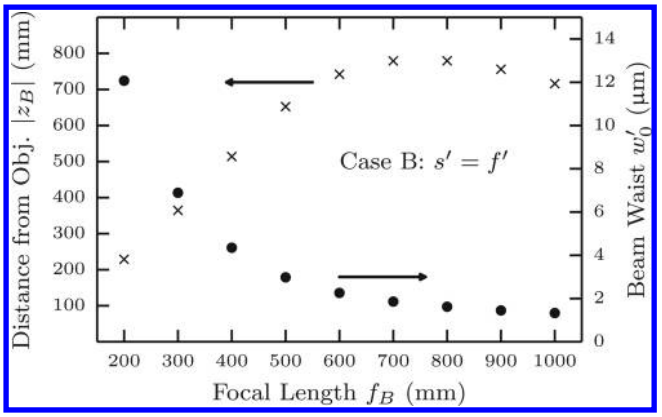

Figure 5. Predicted position z_B (crosses, left axis) of the BFPL as a function of its focal length f_B to ensure focusing of the beam at the focal plane of the ×50 objective, that is, for case B. The corresponding predicted beam waist w'_0 (circles, right axis) are also shown. A fixed laser-to-objective distance of 1560 mm is assumed.

formalism can be used to guide experimental design. Further discussion of what can be learned from this example is provided in Section S.IV. of the Supporting Information.

Continuously Tunable Spot Size. From the results of Figure 5, it is clear that it is not possible to obtain large spot sizes with a BFPL if the lens-to-objective distance is bounded because of space constraints. This problem can be alleviated intuitively by placing a beam expander (BE) before the BFPL in the optical train, which would result in a larger incident beam and a smaller spot at the back focal plane of the objective, and therefore a larger final beam waist. Both commonly used types of beam expanders can be used for this purpose. In both cases, the required distance between the lenses is close to the sum of the focal lengths of the two lenses and the beam magnification is roughly their ratio (again, the Gaussian beam calculations give slightly different values). The Keplerian expander consisting of two convergent lenses has the advantage that the beam can be spatially filtered by positioning a pinhole between the lenses (as implemented in confocal microscopy). The advantage of the Galilean expander with one divergent and one convergent lens is its more compact size.

To reduce the number of optical elements the second lens of the beam expander and the BFPL can be combined into one equivalent convergent lens, resulting in a simple back-focal plane beam-expander (BFP−BE) configuration (Figure 6a) consisting in the case of a Keplerian BE, for example, of only two lenses, one divergent lens (D) followed by a convergent lens (C). We consider the example inspired by our setup and position the convergent lens at the closest allowed distance ($z_C = -600$ mm) with the divergent lens behind it at a tunable distance d_{DC} (i.e., $z_D = z_C - d_{DC}$). We choose a divergent lens with focal length $f_D = -18$ mm and a convergent lens with focal length $f_C = 50$ mm. Self's formalism then predicts that $s' = f'$ ($\Delta = 0$) at two possible values of d_{DC} corresponding to a small and large spot respectively (see Section S.IV. of the Supporting Information for additional details). For the ×50 objective ($f = 3.6$ mm), the first value is $d_{DC} = 32.223$ mm, and the lens combination behaves like a beam expander to enlarge the beam on the objective, which results in a small beam waist of 0.39 µm, close to the diffraction-limited size (and much better than obtained earlier with the objective only). We are here more interested in the other solution, $d_{DC} = 36.787$ mm, which results in a beam waist of $w'_0 = 10.8$ µm, much larger than what

DOI: 10.1021/acs.jpcc.6b04574
J. Phys. Chem. C 2016, 120, 21104−21113

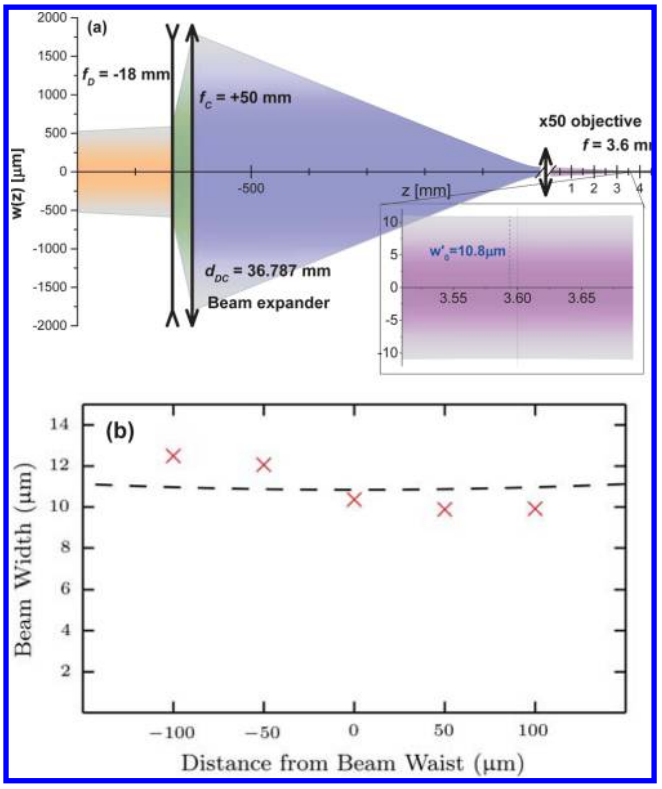

Figure 6. (a) Application of Self's formalism to the use of a two-lens back-focal-plane beam-expander (BFP−BE) combination (f_D = −18 mm, f_C = 50 mm) for a ×50 objective and a BFP−BE-to-objective distance of $|z_C|$ = 600 mm. (b) Predicted beam profile around the image focal plane (dashed line) compared to measured values (symbols) for the same configuration as in (a).

could be obtained with a single BFPL 600 mm away from the objective. Figure 6b shows the predicted beam profile and five measured values for the beam width for this configuration. Similar results are summarized in the top part of Table 3 for other objectives and compared to experimentally determined beam waists, again showing good agreement. Given the small distance between the two lenses, this combination does not occupy much space and can usually be added to existing setups. The beam size is quite sensitive to the exact distance d_{DC}. In order to adjust d_{DC} in practice, it is easiest to minimize the beam divergence (which maximizes beam size) by minimizing the beam spot a distance sufficiently far away from the objective (at least $10f'$).

This configuration can be used to continuously tune the spot size in both cases considered here. In the easier case A, $w'(z = f')$ varies linearly with d_{DC} over a wide range of beam waist (at focal plane) from $w'(z = f')$ = 0.39 µm at d_{DC} = 32.22 mm to $w'(z = f') \approx 20$ µm for $d_{DC} \approx 41$ mm (note the maximum displacement required for the divergent lens is no more than 1 cm). This is shown explicitly in Figure 7, where the validity of the model is again confirmed against experiments.

Table 3. Summary of the Parameters of the BFP−BE Combination for Our Setup and for Various Objectives Using f_D = −18 mm, f_C = 50 or 25 mm, and z_C between −900 and −600 mm[a]

f_C [mm]	$\|z_C\|$ [mm]	objective	d_{DC} [mm]	$w'(f')$ [µm] theor	d_{DC} [mm]	$w'(f')$ [µm] theor/meas
50	600	×10	32.223	1.96	36.911	55.65/61.24
50	600	×20	32.223	0.98	36.832	27.36/26.72
50	600	×20imm	32.223	0.98	36.832	27.36/27.47
50	600	×50	32.223	0.39	36.787	10.84/10.37
50	600	×100	32.223	0.22	36.771	5.40/4.51
50	600	×50	32.223	0.39	36.787	10.84/10.37
50	750	×50	32.235	0.44	35.802	7.67/−
50	900	×50	32.245	0.45	35.156	5.68/−
25	600	×50	7.239	0.78	8.285	5.23/−
25	750	×50	7.270	0.88	8.043	3.68/−
25	900	×50	7.317	1.02	7.849	2.63/−

[a]In each case, the two possible lens distances d_{DC} for which $s' = f'$ are calculated from Self's formalism along with the corresponding predicted waists. Some of those are compared with experimental results.

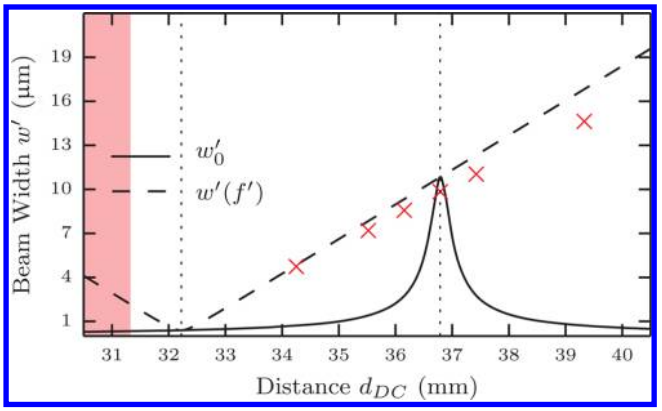

Figure 7. (a) Predicted beam waist w'_0 (dashed line) and beam width at the focal plane $w'(f')$ (solid line) as a function of the distance between the lenses of the BFP−BE combination with the same parameters as in Figure 6. The shaded area indicates that the paraxial assumption is no longer valid. The linear dependence of $w'(f')$ can be used to continuously tune the spot size at the focal plane in case A (Δ would then be nonzero). Two lens positions are relevant to case B (Δ = 0) and are those where the two lines intersect (d_{DC} = 32.223 and 36.787 mm). Symbols indicate experimentally determined values of $w'(f')$.

In the more challenging case B, the condition $s' = f'$ (Δ = 0) can be retained while tuning spot size by changing both the distance between the two lenses and the position of the overall two-lens combination. Self's formalism again proves very useful at estimating required lens positions and predicting spot sizes in this configuration. For example, for f_D = −18 mm and f_C = 50 mm, the beam waist can be varied between 5.7 and 10.8 µm simply by moving the BFP−BE position from z_C = −900 mm to z_C = −600 mm and readjusting d_{DC} to ensure $s' = f'$ (see Table 3). To further extend this tunability one can also replace the convergent lens with a lens of a shorter focal length. For example, for f_C = 25 mm over the same positions, the range of beam waist is 2.6 to 5.2 µm for the larger spot sizes and 0.78 to 1.0 µm for the smaller ones (see Table 3). Overall, using the ×50 objective with the BFP−BE combination with one of those two convergent lenses and varying the position from z_C = −900 to z_C = −600 mm, it is possible to continuously tune the beam waist from ∼0.4 µm to ∼10.8 µm, while retaining (at least approximately) the condition $s' = f$.

DOI: 10.1021/acs.jpcc.6b04574
J. Phys. Chem. C 2016, 120, 21104−21113

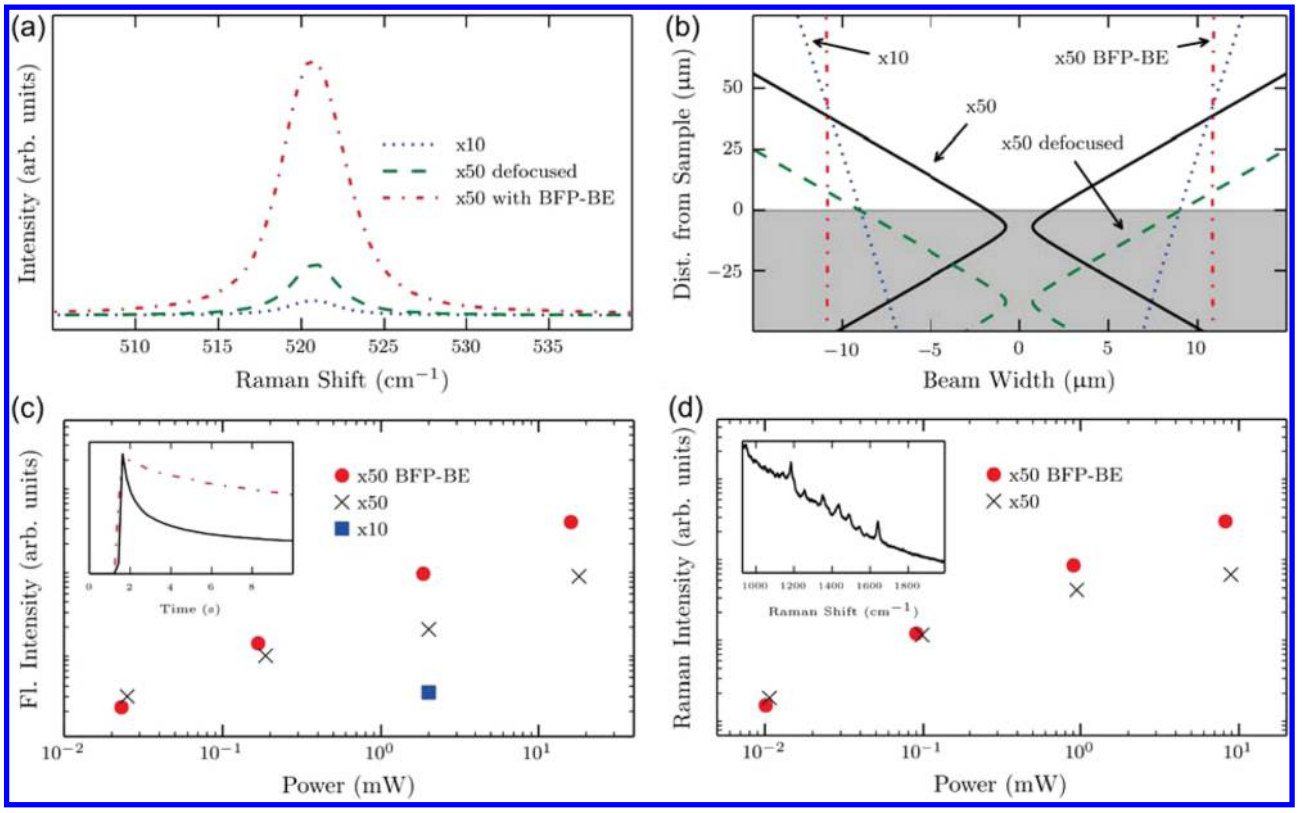

Figure 8. (a) Raman spectrum of Silicon at 514 nm excitation obtained from three micro-Raman configurations achieving large spot sizes (i) with the ×10 objective (spot size 18 μm), (ii) with the ×50 objective but defocused, that is, placing the sample 32 μm away from the beam center to get the same spot size, and (iii) with the same ×50 objective with the BFP−BE combination discussed earlier (spot size 21 μm). The latter spectrum shows the same intensity as without the BFP−BE (not shown) but the spot size is then much smaller (3.6 μm). The corresponding beam profiles are shown schematically in (b). Note that in the ×50 defocused case, the Si/air interface is not in the focal plane of the objective. (c) Effect of spot size on the power dependence of the average fluorescence intensity over 10 s of Rhodamine-B on quartz excited at 514 nm. The inset shows the decay of the signal over time due to photobleaching with (solid line) and without (dashed line) BFP−BE at a power of 2 mW. (d) Effect of spot size on the power dependence of the SERS intensity over 10 s of the 1640 cm^{-1} mode Nile Blue on a gold nanoparticle array[11] excited at 633 nm. The inset shows the Raman spectrum at a power of ∼1 mW.

Application to Fluorescence, Raman, and SERS. We conclude Results: Theoretical Predictions and Experimental Verification by discussing practical examples where the use of large spot sizes, and therefore of the techniques discussed so far, can be particularly beneficial. We focus specifically on fluorescence, Raman, and surface-enhanced Raman spectroscopies. Those examples are presented in Figure 8 and discussed below.

To illustrate the benefits of our approach, we first consider Raman spectroscopy of films, starting with the simplest example: silicon. We focus on a specific experimental configuration based on the same ×50 objective (NA 0.75) as used in the previous examples. The standard spot-size in our system is then predicted and measured to be $2w'(f') = 3.6$ μm. Using the BFP−BE combination, we can increase it to $2w'(f') = 21$ μm. One could argue that the same spot-size could be obtained much more easily by using a lower-magnification objective; for example, for a ×10 (NA 0.25) for which $2w'(f') = 18$ μm. While this is true, the lower NA results in a much lower signal as shown explicitly in Figure 8a,b. Another simple commonly used approach is to defocus the exciting beam. For example, by moving the position of the silicon interface ∼30 μm away from the beam center, a spot size of $2w'$ (30 μm) = 18 μm is obtained, similar to that with the BFP−BE. The problem, however, is that the silicon substrate is no longer at the focal plane of the objective, which affects the collection efficiency of the signal. This is shown explicitly in Figure 8b; it results in a reduced signal by a factor ∼5. Compared to those two alternatives, the use of the BFP−BE combination to increase the spot size results in a much larger signal.

As discussed in the Introduction, larger spot size can be useful for improved spatial averaging and/or to reduce undesirable photoinduced effects such as photobleaching. We will now illustrate the latter in two contexts. First, we consider the fluorescence of a Rhodamine B dye monolayer adsorbed on a quartz slide using a similar procedure[23] (see Section S.I. of Supporting Information for additional details). Contrary to measurements in solutions where the fluorophore can rapidly move in and out of the scattering volume, dye films can be very sensitive to photobleaching, even at relatively small power densities. The use of a larger spot size can then be used to dramatically reduce the power density without reducing the overall signal. This is shown explicitly in the inset of Figure 8c where we compare the fluorescence decay of the Rhodamine B monolayer for the same objective (×50) and same incident power (2 mW) for small and large spot-sizes (and therefore large and small power densities). As expected, the photobleaching decay is much more pronounced for the small spot-size. Large spot sizes are therefore useful to slow down the photobleaching dynamics without compromising on signal intensity. Faster photobleaching decay also translates into lower average intensities. As a result, the power dependence of the

DOI: 10.1021/acs.jpcc.6b04574
J. Phys. Chem. C 2016, 120, 21104−21113

average fluorescence intensity (measured over 10 s) exhibits a saturation/sublinear dependence at a much lower power (and therefore lower signal) with small spot sizes than with large spot sizes (as obtained with the BFP−BE combination), see Figure 8c. As before, a comparable power density could also be achieved by using the ×10 objective, but the signals are then much smaller (square symbol in Figure 8c).

Large spot-sizes can also be exploited in the context of surface-enhanced Raman spectroscopy (SERS), where fixed substrates are commonly used and photobleaching is therefore a common problem.[11,24] Figure 8d highlights this effect again by comparing the small-spot and large-spot power-dependent SERS intensities of the same dye (Rhodamine B) adsorbed on the same gold nanoparticle arrays as studied in ref 11. As pointed out in the latter study, large spot size can moreover be used to ensure a uniform excitation density by limiting the signal collection to a small region around the center of the spot, which is not practical with diffraction-limited spot-sizes.

These example illustrates how the ability to taylor the exciting beam to any desired spot sizes without reducing the signal is paramount for any studies of power-density dependent effects such as photobleaching. It is equally important for any nonlinear spectroscopies, where the power density has a much more dramatic effect on the results than in linear spectroscopies.

DISCUSSION AND CONCLUSION

This work provides a detailed account of how the spot size can be predicted theoretically with practical solutions on how to engineer spot-sizes that are larger than commonly used in fluorescence and Raman microspectrometers. It also provides a clear experimental demonstration that Self's formalism can be used in that context. Although experimental and calculated values for the beam width presented throughout this work are in good agreement, there are obviously discrepancies due to experimental uncertainties, which are intrinsically more pronounced for smaller spot sizes. There are also indications that systematic errors may be present, for example, in Figure 3 or Figure 7. Those could be reduced to some extent by slightly adjusting the Gaussian beam parameters used in the model. It is also possible that the influence of the collection optics/efficiency on the measurement can lead to additional small systematic errors. In any case, those errors remain small and the large set of experimental results presented in this work, compared to prediction, strongly support our main conclusion, namely, Self's formalism for Gaussian beam transformation provides an accurate theoretical prediction of spot size and focal point positions for a wide range of situations relevant to experimental laser spectroscopy.

We have moreover presented this formalism in a self-contained manner and generalized it to experimentally relevant cases such as nonideal Gaussian beam and immersion lenses. This can serve as a reference and, together with the model spreadsheet provided as Supporting Information, form a solid starting point for others to adapt those calculations to other cases of interest. Thanks to this formalism, we have highlighted subtle but experimentally relevant effects even in the most standard configuration, such as an offset between focus of the excitation beam and focal plane of the objective (which as we showed can be easily measured experimentally, providing subtle effects in the imaging of the laser spot are properly accounted for).

Finally, Self's formalism also proves to be an extremely valuable tool for spot-size engineering. With it, we have studied quantitatively simple approaches to obtain larger and tunable spot-sizes, while ensuring if necessary that the image remains located at the focal plane of the objective, which is an important constraint for backscattering configurations. Those results, illustrated here using specific parameters (laser beam properties and distance from microscope), can be readily adapted to other parameters and therefore apply to a vast variety of experimental configurations. This has already guided our experimental design in a number of unrelated recent works[11,13,25] and the simple practical examples discussed here provide additional illustrations of its potential applications. We believe it will prove valuable to other experimenters across varied fields of laser spectroscopy.

ASSOCIATED CONTENT

Supporting Information

The Supporting Information is available free of charge on the ACS Publications website at DOI: 10.1021/acs.jpcc.6b04574.

Additional experimental details and discussions (PDF)

Model spreadsheets implementing Self's formalism calculations on standard configurations (XLSX)

AUTHOR INFORMATION

Corresponding Author

*E-mail: Eric.LeRu@vuw.ac.nz. Phone: +64 4463 5233 x7509.

Notes

The authors declare no competing financial interest.

ACKNOWLEDGMENTS

E.C.L.R. is indebted to the Royal Society of New Zealand (RSNZ) for support through a Rutherford Discovery Fellowship.

REFERENCES

(1) Hess, S. T.; Webb, W. W. Focal volume optics and experimental artifacts in confocal fluorescence correlation spectroscopy. *Biophys. J.* **2002**, *83*, 2300−2317.

(2) Suhling, K.; French, P. M. W.; Phillips, D. Time-resolved fluorescence microscopy. *Photochem. Photobiol. Sci.* **2005**, *4*, 13−22.

(3) Kukura, P.; McCamant, D. W.; Mathies, R. A. Femtosecond stimulated Raman spectroscopy. *Annu. Rev. Phys. Chem.* **2007**, *58*, 461−488.

(4) Jeanmaire, D. L.; Van Duyne, R. P. Surface Raman spectroelectrochemistry Part I. Heterocyclic, aromatic, and aliphatic amines adsorbed on the anodized silver electrode. *J. Electroanal. Chem. Interfacial Electrochem.* **1977**, *84*, 1−20.

(5) Moskovits, M. Surface-enhanced spectroscopy. *Rev. Mod. Phys.* **1985**, *57*, 783−826.

(6) Aroca, R. F. *Surface-enhanced vibrational spectroscopy*; John Wiley & Sons: Chichester, 2006.

(7) Le Ru, E. C.; Etchegoin, P. G. *Principles of surface enhanced Raman spectroscopy and related plasmonic effects*; Elsevier: Amsterdam, 2009.

(8) Webb, R. H. Confocal optical microscopy. *Rep. Prog. Phys.* **1996**, *59*, 427−471.

(9) Dieing, T., Hollricher, O., Toporski, J., Eds. *Confocal Raman microscopy*; Springer: Berlin, 2011.

(10) Eggeling, C.; Widengren, J.; Rigler, R.; Seidel, C. A. M. Photobleaching of fluorescent dyes under conditions used for single-molecule detection: Evidence of two-step photolysis. *Anal. Chem.* **1998**, *70*, 2651−2659.

DOI: 10.1021/acs.jpcc.6b04574
J. Phys. Chem. C 2016, 120, 21104−21113

(11) Galloway, C. M.; Artur, C.; Grand, J.; Le Ru, E. C. Photobleaching of fluorophores on the surface of nanoantennas. *J. Phys. Chem. C* **2014**, *118*, 28820−28830.
(12) Meyer, S. A.; Le Ru, E. C.; Etchegoin, P. G. Combining surface plasmon resonance (SPR) spectroscopy with surface-enhanced Raman scattering (SERS). *Anal. Chem.* **2011**, *83*, 2337.
(13) Meyer, S. A.; Auguie, B.; Le Ru, E. C.; Etchegoin, P. G. Combined SPR and SERS microscopy in the Kretschmann configuration. *J. Phys. Chem. A* **2012**, *116*, 1000.
(14) Le Ru, E. C.; Meyer, S. A.; Artur, C.; Etchegoin, P. G.; Grand, J.; Lang, P.; Maurel, F. Experimental demonstration of surface selection rules for SERS on flat metallic surfaces. *Chem. Commun.* **2011**, *47*, 3903−3905.
(15) Horiba Scientific. *Raman Spectroscopy*; http://www.horiba.com/scientific/products/raman-spectroscopy/raman-spectrometers/, 2016 (accessed May 2016).
(16) Self, S. A. Focusing of spherical Gaussian beams. *Appl. Opt.* **1983**, *22*, 658−661.
(17) Siegman, A. E. How to (maybe) measure laser beam quality. DPSS (diode pumped solid state) lasers: Applications and issues. In *OSA Trends in Optics and Photonics (Optical Society of America)*; Dowley, M., Ed.; OSA Publishing: Washington, DC, 1998; p MQ1.
(18) Siegman, A. E. *Lasers*; University Science Books: Mill Valley, CA, 1986.
(19) Herman, R. M.; Wiggins, T. A. Focusing and magnification in Gaussian beams. *Appl. Opt.* **1986**, *25*, 2473−2474.
(20) Suzaki, Y.; Tachibana, A. Measurement of the μm sized radius of Gaussian laser beam using the scanning knife-edge. *Appl. Opt.* **1975**, *14*, 2809−2810.
(21) Le Ru, E. C.; Blackie, E.; Meyer, M.; Etchegoin, P. G. Surface enhanced Raman scattering enhancement factors: A comprehensive study. *J. Phys. Chem. C* **2007**, *111*, 13794−13803.
(22) Sandison, D. R.; Webb, W. W. Background rejection and signal-to-noise optimization in confocal and alternative fluorescence microscopes. *Appl. Opt.* **1994**, *33*, 603−615.
(23) Tawde, S. R.; Mukesh, D.; Yakhmi, J. V.; Manohar, C. Dye adsorption on self-assembled silane monolayers: optical absorption and modelling. *J. Mater. Chem.* **1999**, *9*, 1847−1851.
(24) Etchegoin, P. G.; Lacharmoise, P. D.; Le Ru, E. C. Influence of photostability on single-molecule surface enhanced Raman scattering enhancement factors. *Anal. Chem.* **2009**, *81*, 682−688.
(25) Hauer, P.; Le Ru, E. C.; Willmott, G. Co-ordinated detection of microparticles using tunable resistive pulse sensing and fluorescence spectroscopy. *Biomicrofluidics* **2015**, *9*, 014110.

DOI: 10.1021/acs.jpcc.6b04574
J. Phys. Chem. C 2016, 120, 21104−21113

Supplementary Information for "Spot Size Engineering in Microscope-based Laser Spectroscopy"

P. Hauer

The MacDiarmid Institute for Advanced Materials and Nanotechnology, School of Chemical and Physical Sciences, Victoria University of Wellington, PO Box 600, Wellington 6140, New Zealand

J. Grand

Université Paris Diderot, Sorbonne Paris Cité, ITODYS, UMR CNRS 7086, 15 rue J-A de Baïf, 75205 Paris Cedex 13, France

A. Djorovic

The MacDiarmid Institute for Advanced Materials and Nanotechnology, School of Chemical and Physical Sciences, Victoria University of Wellington, PO Box 600, Wellington 6140, New Zealand

G. R. Willmott

The MacDiarmid Institute for Advanced Materials and Nanotechnology, Departments of Physics and Chemistry, University of Auckland, Auckland 1010, New Zealand.

E. C. Le Ru

*The MacDiarmid Institute for Advanced Materials and Nanotechnology, School of Chemical and Physical Sciences, Victoria University of Wellington, PO Box 600, Wellington 6140, New Zealand**

* Eric.LeRu@vuw.ac.nz

S.I. SPREADSHEETS FOR GAUSSIAN BEAM CALCULATIONS

An Excel workbook is provided as supplementary file. It contains five spreadsheets to carry out Gaussian beam calculations on standard configurations. The first three relate to

- Focusing of a Gaussian beam by a single lens.
- Focusing of a Gaussian beam by a train of two lenses, with in mind the configuration studied in the manuscript of a BFPL followed by an objective lens.
- Focusing of a Gaussian beam by a train of three lenses, with in mind the configuration studied in the manuscript of a two-lens BFP-BE combination followed by an objective lens.

The two additional spreadsheets are almost identical to the latter two, but are specifically set-up to find the parameters satisfying the condition $\Delta = 0$ (for case **B** of the manuscript) using the built-in solver in Excel. In the BFPL case, this is achieved by varying the BFPL position. In the BFP-BE case, this is achieved by varying the distance between the two lenses of the BE. As evident in the screen shot shown in Fig. S1, those spreadsheets are self-explanatory and contain a diagram defining all parameters. The orange cells can be modified. The most commonly studied outputs are indicated as green cells.

S.II. EXPERIMENTAL SETUP

A Labram HR UV Raman spectrometer (see schematic in Fig. S2) from Horiba Jobin-Yvon was used for all experimental measurements. It is suitable for micro-measurements as it is attached to a Olympus BX41 Microscope, which is equipped with an objective revolver and a CCD camera for sample viewing. The sample position can be adjusted with sub-micrometer precision through a motorized xy-translation stage. Due to space constriction, the BFPL or the two-lens BFP-BE combination have to be positioned in the small region shown in Fig. S3.

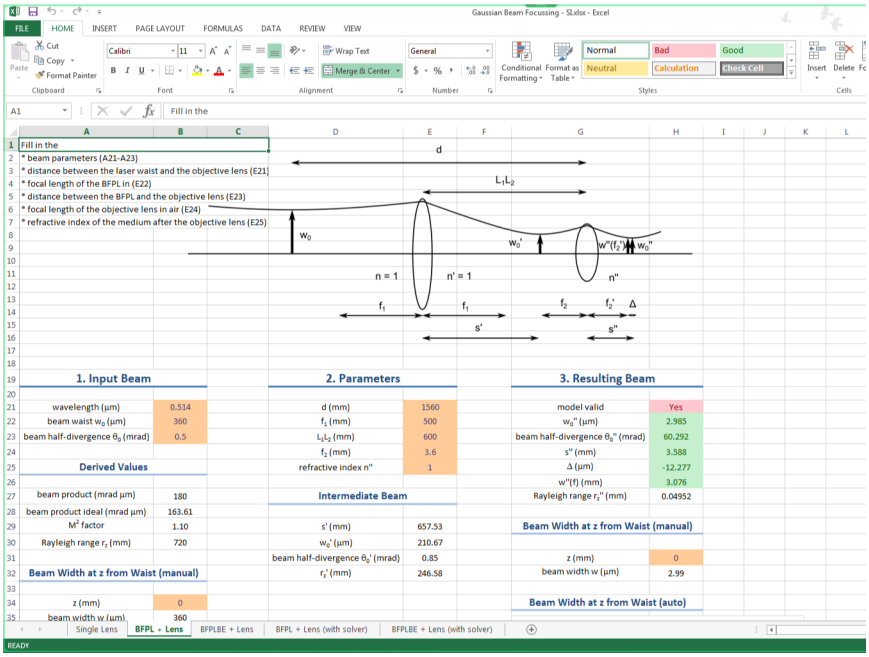

FIG. S1. Screen shot from the Excel spreadsheet modelling the BFP-BE combination.

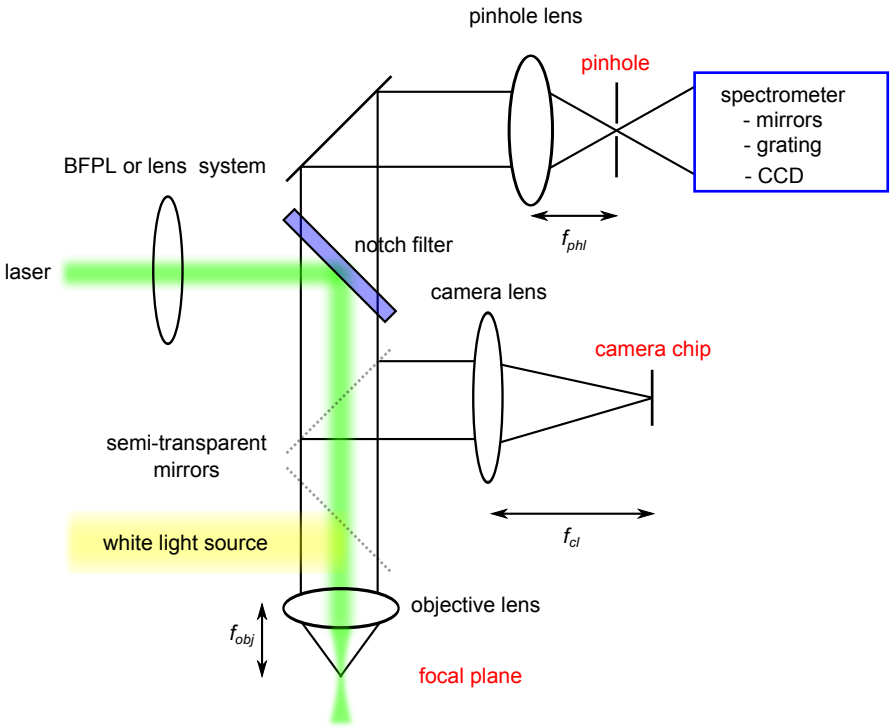

FIG. S2. A schematic layout of our Raman spectrometer. Components in red are conjugated with each other.

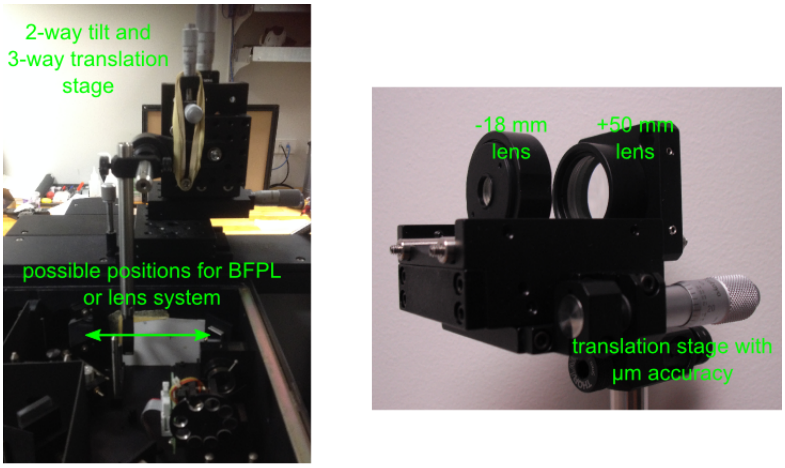

FIG. S3. (a) Installation of a BFPL in our system. The available space is limited to $\sim 15\,\mathrm{mm}$ of the optical beam path, no closer than 600 mm from the objective. (b) The two lenses used in the BFP-BE system are mounted in a contraption to tune the distance between them with μm precision.

S.III. MEASURING Δ, DISTANCE BETWEEN OBJECTIVE AND LASER FOCUS

Measuring the distance between the focal plane of the objective and laser focus appears to be a trivial task. The sample is illuminated both with a white light source and the laser and viewed with a camera and the positions on the vertical adjustment of the microscope table where the sample appears in focus ("white light focus") and where the laser appears to have the smallest size ("apparent laser focus") are noted. However, the position at which the laser spot appears minimal ("apparent laser focus") *does not* coincide in general with the actual position of the beam waist of the focused laser ("real laser focus"). This appears counter-intuitive at first, and it will also depend on the nature of the sample. In our case, we used a highly (specular) reflective sample (silicon). Such a sample creates an image of the incident Gaussian beam, and this image is centered at the mirror image position of the incident beam center. As a result, if the distance from the "white light focus" to the "real laser focus" is Δ (by definition of Δ), then the distance from the "white light focus" to the "apparent laser focus" is in fact $\Delta/2$ (see Fig. S4).

This can be further described by accounting for the way the image is created at the

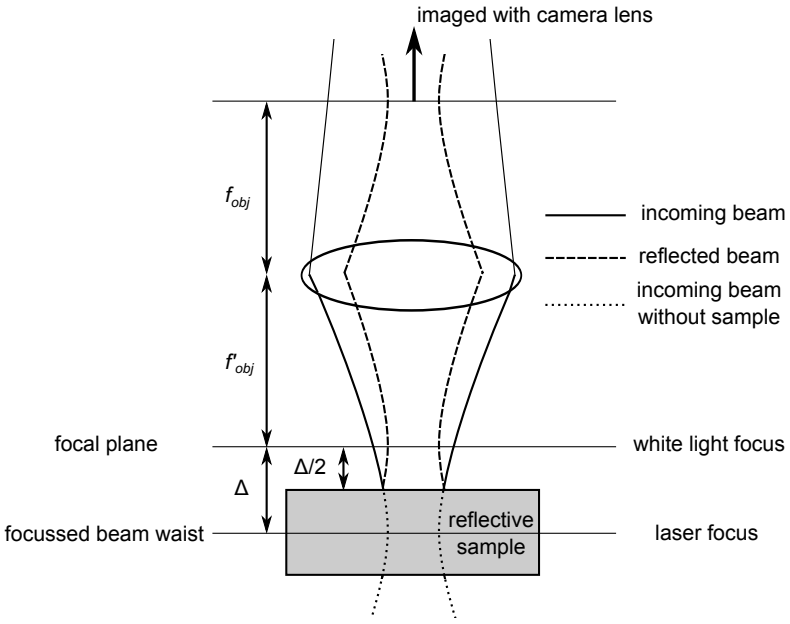

FIG. S4. The incoming an reflected beam when using a highly specular reflective sample.

camera CCD (see Fig. S4). The light collected by the objective is focused onto a camera chip, positioned at the focal plane of the camera lens. As the camera chip is positioned at the focal plane of the camera lens, the beam width at the focal plane is, according to Self's formalism, $\theta'_0 f_{cl}$. The smallest possible spot size is therefore achieved when θ'_0 becomes minimal, which is equivalent to w'_0 being maximum. As the position and size of the incident beam is constant, this occurs when the mirror image of this beam waist is in the focal plane of the objective. The image of the laser spot viewed with such a camera is minimal when the sample is positioned at half the distance between the focal plane of the objective and the actual laser waist. This perhaps counter-intuitive result was confirmed experimentally by measuring the beam waist at different positions along the axis. In this context it has to be noted that a correct positioning of the camera lens is essential to avoid a systematic error in the measurements of Δ. This can be ensured for example by checking that the "white light focus" remains at the same location within a few micrometers when the magnification of the used objective (from the same manufacturer) is changed.

If instead a diffusively reflecting sample is used, the reflected light can be understood as a superimposition of point sources, for which geometric optics can be used. Taking the rays of the collected path into account the position of the "apparent laser focus" will then coincide with the 'white light focus". The "real laser focus" can not be determined in this case.

S.IV. ADDITIONAL DETAILS ON THE BFPL AND BFPL-BE CONFIGURATIONS

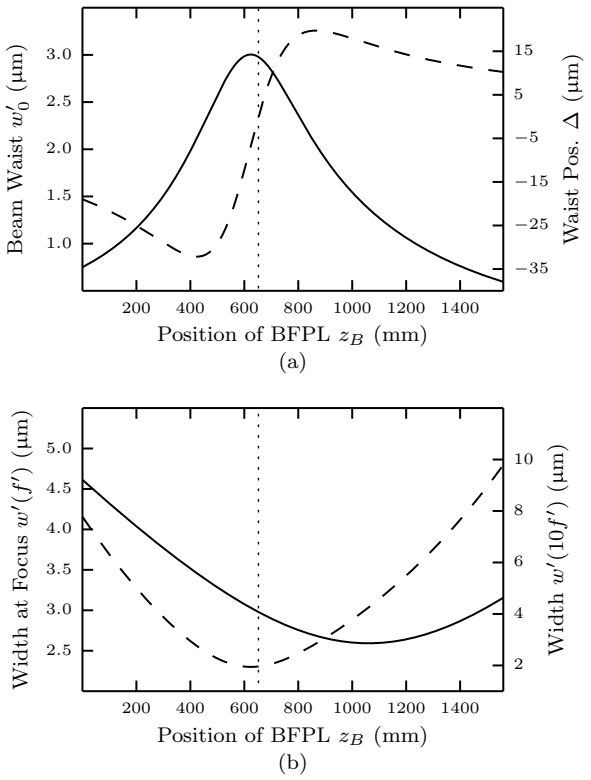

FIG. S5. (a) The size of the beam waist (—) and its position (- -) as a function of the lens distance when a BFPL with $f_B = 500\,\text{mm}$ and an objective lens with focal length 3.6 mm are used. Negative values indicate that the beam waist is located closer to the lens than its focal plane. Note that in order to achieve $s' = f'$, the required distance (vertical line) is not exactly equivalent to the maximum beam waist, which is achieved at a slightly shorter distance. (b) The beam width at the objective focus (—) and at a distance $10f'$ (- -) from the objective lens.

In the BFPL configuration, the spot size and the position of the focused beam waist are quite sensitive to the exact BFPL position (Fig. S5 (a)). Experimentally the correct position for the BFPL can be found by observing the beam beyond the focal plane of the objective lens, where the laser spot is already significantly wider and can easily be viewed by eye (for example at a distance ten times the focal length of the objective lens). By moving the BFPL forward and backward, the optimum position can be found by minimizing the

spot size there (which is equivalent to minimizing the beam divergence). This way, one will achieve a situation which does not exactly result in $s' = f$ but is close enough for most purposes. By simply observing the spot in the focal plane one would not be able to find the correct position of the BFPL as the size of the beam width depends approximately linearly on the distance between the lenses close to the critical position (Fig. S5 (b)). This, however, is also of advantage as the spot size at the focal plane, which is the relevant parameter in most experiments, is relatively insensitive and also tunable with the position of the BFPL.

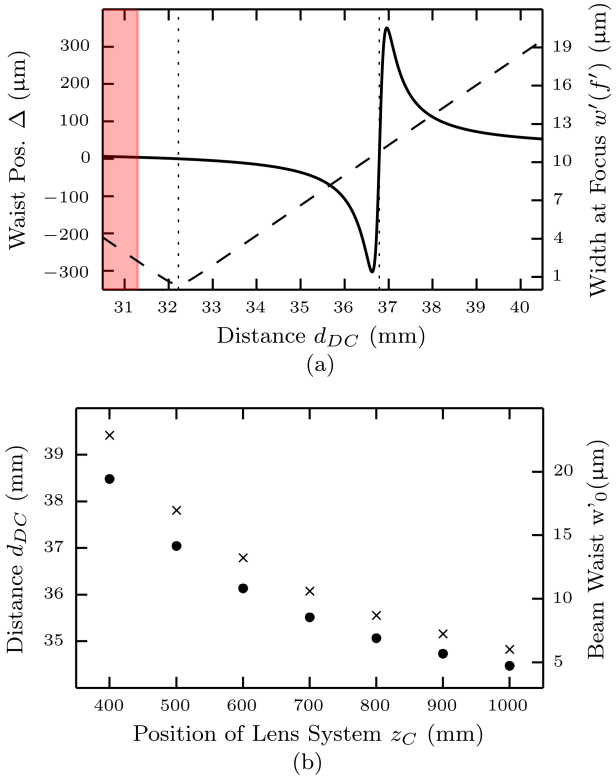

FIG. S6. (a) Predicted offset Δ solid line, left axis) and beam width at the focal plane $w'(f')$ (dashed line, right axis) as a function of the distance $|d_{DC}|$ between the two lenses of the BFP-BE combination using a fixed BFP-BE-to-objective distance of $|z_C| = 600\,\text{mm}$ and a $\times 50$ objective. The shaded area indicates that the paraxial assumption is no longer valid. The vertical dotted lines indicate where $\Delta = 0$. (b) The required distance $|d_{DC}|$ (crosses, left axis) between the two lenses of the BFPL-BE in order to achieve the situation in case **B** ($\Delta = 0$) and the resulting beam waist (circles, right axis) as a function of the the BFP-BE-to-objective distance z_C.

In the BFP-BE configuration, the correct distance $|d_{DC}|$ between the two lenses that

fulfills the condition $\Delta = 0$ (case **B**) and produces the largest spot size can be found experimentally in a similar fashion as explained above. To achieve the smallest spot size, i.e. use the lens combination as an actual beam expander, $|d_{DC}|$ has to be adjusted to the distance where the spot size appears minimal when observing the spot through the objective (Fig. S6 (a)). When the constraint $|z_C|$ =constant is lifted, the spot size can be continuously tuned over a wide range while retaining the condition $\Delta = 0$ by adjusting $|d_{DC}|$ accordingly (Fig. S6 (b)).

S.V. SUPPLEMENTARY METHODS: SAMPLE PREPARATION FOR FLUORESCENCE

The Rhodamine B dye monolayer was prepared according to the following modification of the procedure introduced by Tawde et al. [1]. A self-assembled monolayer of phenylsilane was first deposited onto a clean, pre-prepared, hydrophilic quartz substrate. A 2 mM solution of trichlorophenylsilane (Sigma Aldrich, $\geq$ 97%) in a 7:6 (volume-volume ratio) toluene/chloroform mixture was prepared in a beaker under a nitrogen atmosphere. After this initial silanization of the glass beaker walls, the solution was discarded and re-made in the same beaker to preserve a well-defined silane concentration. Note that both the toluene and chloroform need to be anhydrous due to the high reactivity of trichlorophenylsilane with water. The silane film was deposited by dipping the quartz substrate into the prepared silane solution for 10 mins under sonication and then left to stand in the solution for a further 45 minutes. The substrate was then removed, dried with a jet of nitrogen and cured for 15 minutes at 50°C. The substrate was then left to cool for 15 minutes then dipped into a beaker with a 100 μM solution of Rhodamine B in deionised water (Ultrapure MilliQ). The beaker was then covered with Parafilm and left to stand 24 hours, upon which the substrates were removed from solution and the excess dye was washed off by rinsing with deionised water then patted down with a Kimwipe. The backside of the films was cleaned with toluene to remove any adsorbed silane and Rhodamine B. The prepared films show a very light pink

color.

---

[1] S. R. Tawde, D. Mukesh, J. V. Yakhmi, and C. Manohar, "Dye adsorption on self-assembled silane monolayers: optical absorption and modelling," J. Mat. Chem. **9**, 1847–1851 (1999).